Study of in-plane electrical transport anisotropy of a-axis oriented YBa$_2$Cu$_3$O$_{7-\delta}$ nanodevices

Reza Baghdadi,[1] Riccardo Arpaia,[1] Evgeny Stepantsov,[2] Marco Arzeo,[1] Dmitri Golubev,[3] Domenico Montemurro,[1] Eric Andersson,[1] Thilo Bauch,[1] and Floriana Lombardi[1, *]

[1]*Quantum Device Physics Laboratory, Department of Microtechnology and Nanoscience,*
Chalmers University of Technology, SE-41296 Göteborg, Sweden
[2]*Shubnikov Institute of Crystallography, Russian Academy of Sciences, Leninskii pr. 59, Moscow, 119333 Russia*
[3]*Low Temperature Laboratory (OVLL), Aalto University School of Science, P.O. Box 13500, FI-00076 Aalto, Finland*
(Dated: April 10, 2017)

In the present work, we report the growth of fully untwinned high quality a-axis oriented YBa$_2$Cu$_3$O$_{7-\delta}$ films on (100) SrLaGaO$_4$ substrates using PrBa$_2$Cu$_3$O$_{7-\delta}$ as a buffer layer. We have also fabricated nanowires at different angles γ with respect to the [0,1,0] direction of the substrate and studied the in-plane anisotropy of the critical current density, which we explained by considering the anisotropy in the coherence length ξ and London penetration depth λ_L. Finally, half-integer Shapiro-like steps measured in slightly underdoped c-axis oriented ($\gamma = 90°$) nanowires point towards a different transport regime, which could shed light on intriguing issues of high critical temperature superconductors (HTS).

I. INTRODUCTION

a-axis thin films of High critical Temperature Superconductors (HTS) are very interesting systems which give direct access to the study of the anisotropy of the superconducting transport properties in these compounds. At the beginning of the 90's, a-axis YBCO films attracted much attention because of the possibility to employ the longer a-b planes coherence length, ξ_{ab}, for the realization of multilayer based Josephson devices [1, 2]. Nowadays, with the advancement of the nanotechnologies applied to HTS, YBCO a-axis films would represent the natural choice for the realization of superconducting proximity based hybrid systems such as superconductor-normal conductor-superconductor (SNS) junctions. The direct contact of the a-b plane with the normal conductor would allow a stronger induced superconductivity in proximity based devices, due to the high value of the superconducting gap. This is of particular relevance in devices where the normal conductor is an exotic material characterized for example by a Dirac dispersion. In such hybrids the d-wave order parameter and the high critical field of HTS could be instrumental to get devices with new functionalities [3, 4].

However, the growth of high quality epitaxial a-axis YBCO thin films has resulted to be more complicated than the c-axis counterpart. This is mostly due to the lower deposition temperature, involved in the nucleation of a-axis grains, compared to c-axis ones [5], which leads to films with a generally lower critical transition temperature and poorer crystallinity [6]. While (110) NdGaO$_3$ substrates [7] have been successfully employed to grow a-axis films, the most reproducible results have been obtained by using a buffer layer technique. YBCO

buffer layers deposited at lower temperature on (100) SrTiO$_3$ and LaAlO$_3$ substrates [8, 9] resulted in good quality but twinned a-axis films. The best reports refer instead to a-axis films grown on PrBa$_2$Cu$_3$O$_{7-\delta}$ (PBCO) buffer layer on (100) SrLaGaO$_4$ (SLGO) substrates [10–17], that are also untwinned. Moreover a-axis films have much smaller grains than c-axis films [2], which can give rise to rougher surfaces and complications in the realization of multilayer structures. As a matter of fact the nanopatterning of a-axis films has also resulted quite challenging. At present YBCO nanowires fabricated on c-axis films [18, 19], show properties close to the as grown films, while there are no reports on nanodevices fabricated starting from a-axis thin films.

In this paper we present the first measurements on nanowires and nano superconducting quantum interference devices (nanoSQUIDs) patterned on untwinned a-axis YBCO films with width down to 65 nm and oriented at different in-plane angles γ with respect to the [0,1,0] direction of the SLGO substrate. From the measurements of the resistive transition as a function of temperature, of the critical current density of the nanowires and of the critical current modulation of the nanoSQUIDs as a function of an externally applied magnetic field, we get information about the anisotropy of the coherence length, ξ, and of the London penetration length, λ_L, of YBCO when the dimensionality of the systems is strongly reduced. For example nanowires oriented along the YBCO c-axis direction ($\gamma = 90°$) are characterized by a series of confined a-b planes with nanoscale dimensions: these systems act as an array of rather weakly coupled superconducting nanodots, of relevance for a number of applications [20–22]. At the same time, such kind of structure can inspire future work aimed at studying the effect of the confinement of the a-b planes on the appearance of the recent discovered charge density wave order [23–25] and its interplay with high critical temperature super-
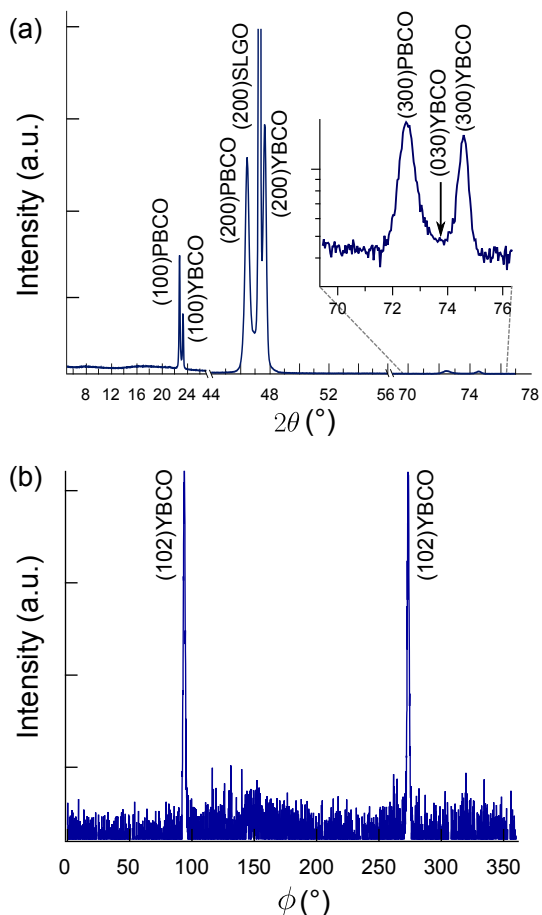
* floriana.lombardi@chalmers.se

FIG. 1: a) 2θ-ω XRD scan of a 50 nm thick a-axis YBCO film grown on a (100) SLGO substrate, by using a 200 nm thick, a-axis oriented, PBCO layer as a buffer. Only the $(\ell00)$ reflections related to a a-axis orientation of the YBCO unit cell are present, as highlighted in the inset. b) XRD ϕ-scan of the YBCO (102) reflections: only two peaks, at 90° and 270°, are observed, confirming the untwinned nature of our a-axis YBCO films.

conductivity.

II. CHARACTERIZATION OF THE A-AXIS YBCO FILMS

To promote the growth of a-axis YBCO films, we have used a 200 nm thick PBCO buffer layer, deposited by rf sputtering (rf power = 50 W, T = 830 °C, p_{O_2} = 0.1 mbar) on top of a SLGO(100) substrate. The sample is then transferred *in situ* to the pulsed laser deposition (PLD) chamber, where a YBCO film (thickness t = 50 nm) is deposited at a temperature of 790 °C, in a 0.82 mbar O_2 atmosphere. While the sample is heated to reach the deposition temperature, the O_2 pressure is kept at 300 Torr, to avoid oxygen out diffusion from the PBCO layer which could favor the nucleation of c-axis
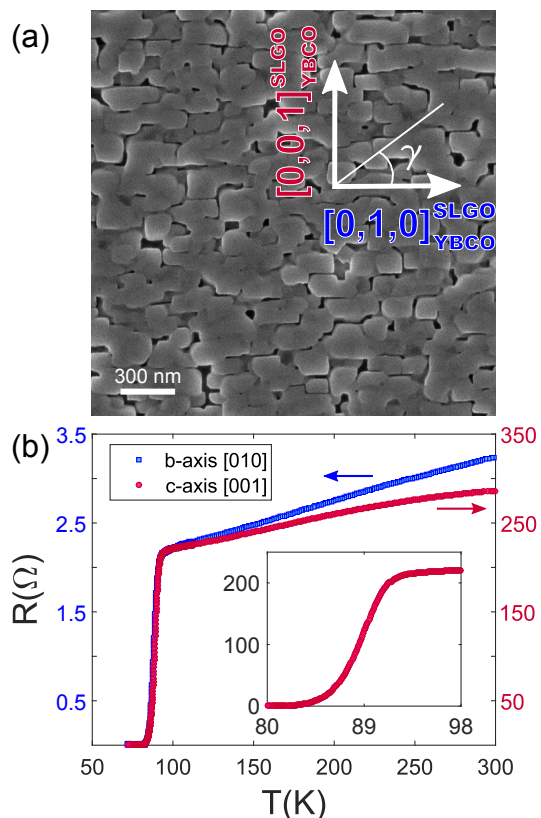

FIG. 2: a) SEM picture of an a-axis YBCO film. b) The $R(T)$ of a film, measured both along the [0,1,0] (blue squares) and [0,0,1] (red circles) YBCO direction. The critical temperature T_C, calculated as the maximum of dR/dT, is ≈ 88 K, as highlighted in the inset.

domains in the YBCO layer.

The structural properties of the films have been analyzed by X-ray diffraction (XRD). In the symmetrical 2θ-ω scans, only the $(\ell00)$ reflections of YBCO - in addition to the $(\ell00)$ reflections of the PBCO buffer layer - are observed (see Fig. 1(a) and inset therein), confirming that the films are highly crystalline, and purely a-axis oriented. To explore the in-plane texture of these films, ϕ scans of the (102) YBCO reflections have been performed. Only two peaks are present, with a symmetry of 180° (see Fig. 1(b)): this evidence confirms that the b-axis and the c-axis of the YBCO are totally detwinned, in agreement with the best results on a-axis YBCO films previously reported in literature [26, 27].

The morphology of the films has been analyzed by means of scanning electron microscopy (see Fig 2(a)): a granular structure is visible, characterized by elongated domains, typical of a-axis films [28], oriented along the [0, 1, 0] YBCO direction (b-axis).

The resistance versus temperature $R(T)$ of a typical thin a-axis film is shown in Fig. 2(b), both along the b-axis (blue squares) and the c-axis (red squares) direction. In the normal state, a strong anisotropy is present:

the resistance in the c-axis direction is ≈ 100 times larger than in the the b-axis direction just above the superconducting transition, in agreement with earlier reports on untwinned YBCO single crystals [29, 30]. The behavior of the resistance with the temperature is also anisotropic: along the b-axis, the resistance shows a linear temperature dependence from 300 K down to the superconducting transition, which is typical of optimally doped films [31]; along the c-axis, the range of linearity decreases, and a downward bending of the resistance with the temperature, resembling that of an underdoped YBCO c-axis film, develops at low temperatures. Finally, we have recorded a critical temperature $T_C \approx 88$ K along both the YBCO in plane directions, calculated as the temperature where the derivative dR/dT is maximum, and a transition broadening $\Delta T_C \approx 3$ K.

III. NANOSTRUCTURES TO STUDY THE IN-PLANE LONDON ANISOTROPY

To study the in-plane anisotropy of the critical current density in a-axis oriented YBCO films, at dimensions comparable with the fundamental superconducting lengths (λ_L, and ξ), we have patterned, on the same chip, nanostructures (nanowires and Dayem bridge nanoSQUIDs) at different in-plane angles γ with respect to the [0,1,0] direction of the substrate.
The patterning has been done by using a diamond like carbon mask in combination with electron beam lithography and a very gentle ion-beam etching. More details on the nanofabrication can be found elsewhere [18, 19]. We have fabricated nanowires, protected by a Au capping layer, with widths w down to 65 nm and lengths $l = 1.5w$ (see SEM image in Fig. 3(a)). The transport properties of the nanowires have been investigated via current-voltage (IV) characteristics at $T = 4$ K and resistance versus temperature $R(T)$ measurements. In our 4-point measurement setup, the current and voltage probes are located at the far ends of the two wide and long electrodes, connected in series to each nanowire. The supercurrent in nanowires aligned along the b-axis direction (which in our convention corresponds to $\gamma = 0°$) is carried by the a-b planes as illustrated in Fig. 3(b), while for those patterned along the c-axis direction ($\gamma = 90°$) the current flows through an array of weakly coupled nanosized CuO_2 planes (see Fig. 3(c)).

Fig.4(a) shows the extracted critical current density, $J_C = I_C/(w \cdot t)$ for 65 nm and 140 nm wide nanowires patterned at different in-plane angles γ. An anisotropy of the critical current density is clearly visible, with a maximum for $\gamma = 0°$, and a reduction by one order of magnitude approaching $\gamma = 90°$ where the current flows entirely along the c-axis. We shall show that this dependence of the J_C values on γ is a consequence of the anisotropy of the coherence length and of the London penetration depth in the a-b plane and in the c-axis direction. For thin ($t < \lambda_L$) and narrow wires ($4.4\xi \leq w < \lambda_L^2/t$) the

critical current density is limited by Abrikosov vortices overcoming the vortex entry edge barrier [32, 33]. Considering an anisotropic thin superconductor and applying the approach discussed in Ref. [32], one can calculate the critical current densities for such a wire oriented along the b-axis ($\gamma = 0°$)

$$J_C^b \propto \frac{\Phi_0}{\lambda_b \lambda_c \xi_c}, \tag{1}$$

and for a wire oriented along the c-axis ($\gamma = 90°$)

$$J_C^c \propto \frac{\Phi_0}{\lambda_b \lambda_c \xi_b}, \tag{2}$$

with a ratio $\frac{J_C^c}{J_C^b} = \frac{\lambda_L^b}{\lambda_L^c}$, where we used the property $\xi_c/\xi_b = \lambda_L^b/\lambda_L^c$ [34]. Here, the product $\lambda_b \cdot \lambda_c$ in the dominator of Eqs. (1) and (2) reflects the fact that the circulating screening current of the Abrikosov vortex is flowing in the $[1\,0\,0]$ planes of the crystal. i.e. along the b- and c-axis. In Eqs. (1) and (2), the relevant coherence length is along the direction of the vortex entry path which is perpendicular to the current flow.

In the case of our nanostructures one can easily show that the $J_C(\gamma)$ follows the relation [34, 35]:

$$J_C(\gamma) = \frac{J_C^b}{\sqrt{(\cos^2 \gamma + (\frac{\lambda_L^c}{\lambda_L^b})^2 \sin^2 \gamma)}} \tag{3}$$

where J_C^b is the critical current density for $\gamma = 0°$, and λ_L^c and λ_L^b are the London penetration depths along c-axis and b-axis, respectively.

The in-plane London anisotropy ratio λ_L^c/λ_L^b can be estimated from the magnetic field response of Dayem bridge nanoSQUIDs implementing nanowires oriented either along b-axis or along c-axis (see Fig.4(c)). In this configuration, the nanoSQUID loop is formed by two 65 nm wide nanowires connecting two micron-sized electrodes. For such geometry, the total loop inductance L_{loop} is mainly dominated by the kinetic contribution, depending on both λ_L^b and λ_L^c. From the critical current I_C modulation as a function of the externally applied magnetic field B measured at $T = 4$ K, the total loop inductance L_{loop} can be experimentally determined as $L_{loop}^{exp} = \Phi_0/\Delta I_C$, where Φ_0 is the magnetic flux quantum and ΔI_C is the difference between the maximum I_C^{max} and the minimum I_C^{min} values of the critical current. Therefore we have determined the in-plane London anisotropy by comparing the experimentally obtained L_{loop}^{exp} with the total loop inductance L_{loop}^{num}, which is numerically calculated by solving the Maxwell and London equations for each of the two SQUID geometries [36–38], and using λ_L^b and λ_L^c as the only two fitting parameters. We have obtained a very good agreement between L_{loop}^{exp} and L_{loop}^{num} in both the geometries assuming that $\lambda_L^b = 280$ nm and $\lambda_L^c = 4.2$ μm. In particular, the λ_L^b value is very
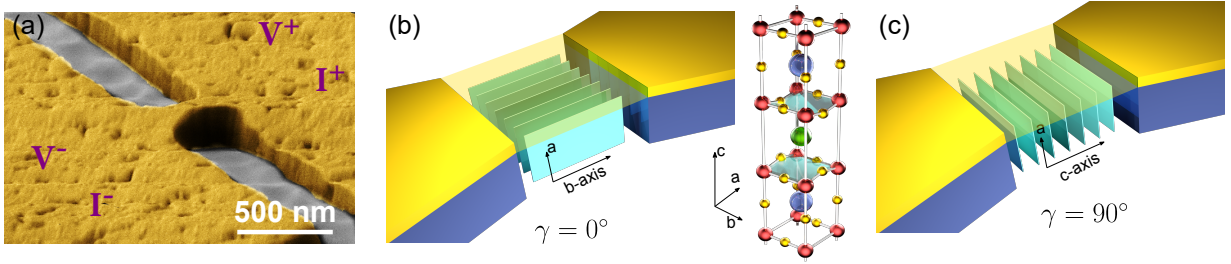
FIG. 3: a) SEM picture of a 65 nm wide a-axis YBa$_2$Cu$_3$O$_{7-\delta}$ nanowire covered by a 50 nm thick Au layer. b) Schematic representation of a b-axis aligned YBCO nanowire, where the current flowing from one electrode to the other is in the a-b planes. c) Schematic representation of a c-axis aligned YBCO nanowire in which the current flows perpendicularly to the weakly coupled a-b planes.
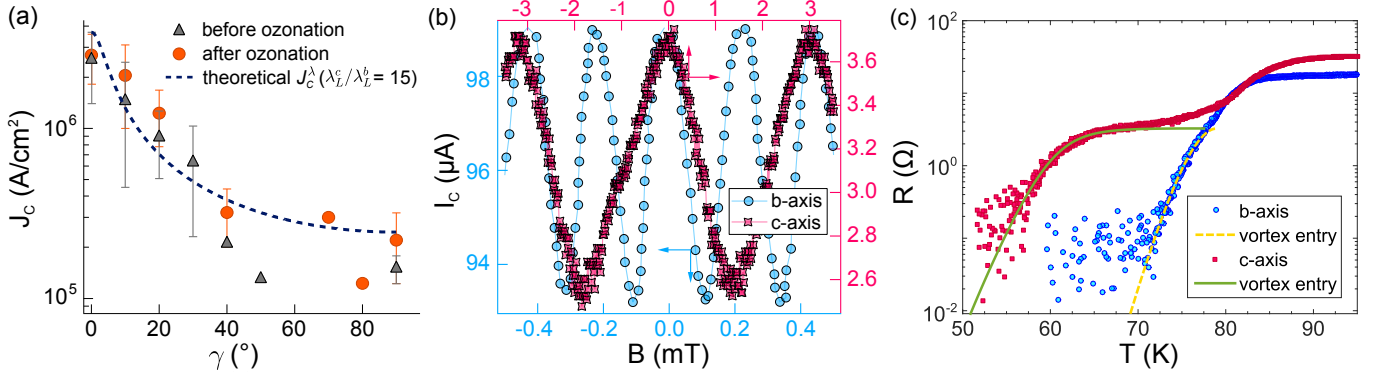

FIG. 4: a) Average critical current density J_C vs the angle γ for the 65 nm and 140 nm wide YBCO nanowires before (gray triangles) and after (orange circles) the ozone treatment. For each angle, the error bar, related to the broadening of the distribution of the J_C values measured on identical nanowires, is equal to 2σ. The theoretical J_C^λ related to a London anisotropy $\lambda_c/\lambda_b = 15$ is shown as a dotted line. b) Critical current modulation as a function of an externally applied magnetic field for b-axis aligned (blue circles) and c-axis aligned (red squares) 65 nm wide Dayem bridge nanoSQUIDs at $T = 4.2$ K. The loop inductances L_{loop}^b and L_{loop}^c, extracted from the critical current modulation depth, are 0.3 nH and 1.7 nH. c) Resistance versus temperature measurement of 65 nm wide nanowires, oriented along the b-axis (blue circles) and the c-axis (red squares) direction. The solid lines are the fits, considering a thermally activated vortex-entry model.

close to the one of the YBCO in-plane London penetration depth λ_L^{ab} extracted in nanostructures patterned on c-axis films [33, 37, 39].

Given the London anisotropy ratio $\lambda_L^c/\lambda_L^b \approx 15$ from the $I_C(B)$ modulations, we have evaluated the expected $J_C(\gamma)$ through equation (3)(see the dashed line in Fig.4(a)). The expected dependence of J_C on γ is in good agreement with the measured behavior up to $\gamma = 40°$ [40]. Above this value the observed deviation could be indicative of the oxygen out-diffusion from the oxygen chains along the b-axis. This effect starts to play a crucial role as soon as a substantial number of CuO chains, included in the nanostructure, become exposed to the environment on one lateral side of the nanowires (while the Au capping minimizes the oxygen out-diffusion from the top of the nanostructures). Obviously the oxygen loss becomes more dramatic for c-axis oriented nanowires when the CuO chains along b-axis are equally exposed on both sides of the nanowire. One

can therefore expect that these structures (nanowires at $\gamma = 90°$) can have a different doping level.

To strengthen our findings of a strong role of the in-plane anisotropy of the London penetration depth in the transport properties of nanostructures, we have measured the $R(T)$ of 65 nm wide nanowires, patterned at $\gamma = 0°$ and $\gamma = 90°$ (see Fig. 4(c)). As a consequence of the chosen geometry (see Fig. 3(a)), the first, sharper, drop of resistance at higher temperatures represents the transition of the wide electrodes, while the second, broader, transition is attributed to the nanowire. The broadening of the nanowire resistive transition as a function of temperature, $R(T)$, can be analyzed, both along the b-axis and the c-axis, in terms of a thermally activated vortex-entry model [32, 33, 41], valid for structures having width much larger than the superconducting coherence length ($w \gg 4.4\xi(T)$ up to $T \approx T_C$). According to this model, the broadening of the superconducting transition, which

is a consequence of the Abrikosov vortices, perpendicular to the bias current, crossing the nanowire, can be expressed as [33, 42]

$$R_v(T) = 7.1 R_\square \frac{l\xi(T)}{w^2} \left(\frac{\epsilon_0(T)}{k_B T}\right)^{3/2} \exp\left[-\frac{\epsilon_0(T)}{k_B T} \ln\frac{1.47w}{\pi\xi(T)}\right]$$
(4)

where $R_\square$ is the sheet resistance of the wire, k_B is the Boltzmann constant, and $\epsilon_0(T) = \Phi_0^2 t/4\pi\mu_0\lambda_L^2(T)$ is the characteristic energy giving the magnitude of the potential barrier for the vortex entry. Equation (4) depends on both the London penetration depth λ_L and the superconducting coherence length ξ. Here we have extended the model reported in Ref. [33] considering an anisotropic superconductor. In this case Abrikosov vortices crossing a-axis film nanostructures have an elliptic-like normal core shape [43]: in Eq. (4) we have therefore defined an effective London penetration depth $\lambda_L^2 = \lambda_b \cdot \lambda_c$ for the nanowires oriented both along b- and c-axis direction. The coherence length in Eq. (4) has to be taken perpendicular to the current flow direction in the nanowire. This means that for b-axis aligned nanowires the coherence length is given by the one along the c-axis ($\xi = \xi_c$) and for c-axis aligned wires it is given by the one along the b-axis ($\xi = \xi_b$). For the temperature dependencies of the London penetration depth and of the coherence length we use the following common approximations $\lambda_L^2(T) = \lambda_b(0)\lambda_c(0)/(1-T^2/T_C^2)$ and $\xi_{b,c}^2(T) = \xi_{b,c}^2(0)/(1-T^2/T_C^2)$ [33], where $\lambda_b(0)$, $\lambda_c(0)$ and $\xi_{b,c}(0)$ represent the zero-temperature values.

We have fitted the broadening of the superconducting transition of both the $\gamma = 0°$ and $\gamma = 90°$ nanowires as

$$R(T) = \left[R_v^{-1}(T) + R_{sh}^{-1}(T)\right]^{-1}$$
(5)

including the resistive shunt R_{sh} of the Au capping layer in addition to the vortex entry resistance (see solid lines in Fig. 4(c)). For the fitting procedure, we used the values $\lambda_b(0)$ and $\lambda_c(0)$ obtained from the nanoSQUID measurements as fixed parameters. By considering nanowire dimensions very close to the geometrical ones (see Table I), we have found a very good agreement of our experimental data with the model. The extracted zero tem-

TABLE I: Summary of the fixed and extracted fit parameters of the b-axis and c-axis oriented nanowires shown in Fig. 4(c), using a thermally activated vortex entry model [eqs. (4) and (5)]

Nanowire	t (nm)	l (nm)	w (nm)	T_C (K)	$R_\square$ (Ω)	R_{sh} (Ω)	$\xi_b(0)$ (nm)	$\xi_c(0)$ (nm)	$\lambda_b(0)$ (nm)	$\lambda_c(0)$ (μm)
[0,1,0]	45	100	55	80.4	80	8.5	—	0.55	280	4.2
[0,0,1]	45	100	45	80.0	250	3.3	2.8	—	280	4.2

perature superconducting coherence length, $\xi_b(0)$ value (2.8 nm) is very close (see Table I) to the ones reported in literature and associated to nanostructures patterned on c-axis films [33, 39, 42]. The anisotropy ratio

$\xi_b(0)/\xi_c(0) \approx 5$ is lower than that of the London penetration depths: this could be due to the uncertainty in the specific temperature dependence of ξ_c and λ_c that we have assumed to be similar to ξ_b and λ_b, and/or to the oxygen out-diffusion from the exposed oxygen chains, giving rise to slightly underdoped nanostructures.

IV. HALF-INTEGER SHAPIRO-LIKE STEPS IN UNDERDOPED A-AXIS NANOWIRES UNDER MICROWAVE RADIATION

To restore the oxygen content in the more de-oxygenated nanostructures, we have annealed the sample for 2 hours at 150 °C in a chamber filled with ozone, with a procedure already successfully used for nanowires patterned on c-axis YBCO films [42, 44]. As a consequence of this treatment, the critical currents of the nanowires increase up to a factor 2-3 (see circles in Fig.4(a)).

To get more insights into the transport along the c-axis, in a regime of strong confinement of the a-b planes, we have studied the phase dynamics of the c-axis nanowires, by applying microwave radiation. As a consequence of the synchronization between the frequency of vortex entry and that of the applied microwave f_{MW}, Shapiro-like steps at $V_n = n\frac{hf_{MW}}{2e}$ appear in the IV characteristics [45–48].

Here, our focus is on c-axis oriented nanowires, since the b-axis oriented ones show the expected integer Shapiro-like steps both before and after ozonation. Fig. 5(a) shows the logarithmic differential resistance map as a function of the device bias current and of $P^{\frac{1}{2}}$ (where P is the applied microwave power at the output of the microwave source) at $f_{MW} = 5.4\,\text{GHz}$, before ozonation. We observe both the integer and the half-integer Shapiro-like steps, as shown in the $\frac{dI}{dV}$ vs V plot (Fig. 5(c)). Interestingly, the half-integer Shapiro-like steps get significantly suppressed after the ozone treatment of the sample (Figs. 5(b) and 5(d)).

The presence of half-integer Shapiro-like steps in the IV characteristics is rather intriguing. The fact that they disappear with the ozonation of the nanowire strongly points towards a different superfluid transport regime in the underdoped region of the HTS phase diagram. For underdoped HTS there are several theoretical proposals [49, 50] predicting the existence of a $4e$ superfluid component in parallel with a conventional $2e$ one. In this case the $4e$ component would give half-integer Shapiro-like steps caused by half-integer Abrikosov vortices.

However, the confinement of the a-b planes in c-axis nanowires and low oxygen content could also play a role possibly reducing the strength of coupling between the planes. For such a scenario a Josephson coupling between the planes (in analogy with $Bi_2Sr_2CaCu_2O_{8+x}$ samples) [51] could explain the appearance of half-integer Shapiro-like steps. Indeed c-axis nanowires would behave like an array of high transparent Josephson junctions with high order harmonics in the current phase relation, leading
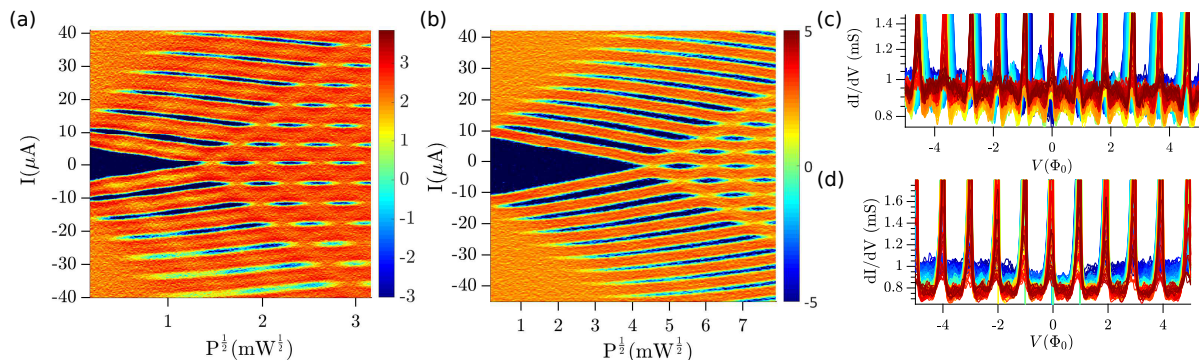
FIG. 5: Color maps of differential resistance as a function of junction DC bias and radiated microwave field amplitude $P^{\frac{1}{2}}$ at $T = 5\,\mathrm{K}$ for a c-axis orientated nanoSQUID a) before ozone treatment and b) after ozone treatment,c) the conductance plotted as a function of $V(\Phi_0)$ before the ozone treatment, and d) the same measurement after the ozone treatment. The half-integer steps vanished after the sample is oxygenated in the ozone chamber.

to fractional Shapiro steps. After ozonation the coupling between the planes increases and the transport will be dominated by vortex-entry with a specific frequency which at the locking with the microwave radiation gives only integer Shapiro steps (see Fig. 5(d)).

Whatever scenario realizes in our c-axis nanowires, our study clearly highlight the potentialities of these nanostructures to study fundamental issues of high critical superconductivity.

V. CONCLUSIONS

In conclusion, we have grown 50 nm thick a-axis oriented YBa$_2$Cu$_3$O$_{7-\delta}$ films on (100) LaSrGaO$_4$ substrates using PrBa$_2$Cu$_3$O$_{7-\delta}$ as a buffer layer. The crystal structure and the morphology of our films has been analyzed by XRD and SEM, from which we conclude that the films are fully untwinned. The in-plane anisotropy of the properties, already observed in the normal state from resistivity measurements on unpatterned films, has been further studied in the superconducting state in nanostructures, with widths down to 65 nm, that we have patterned at different angles γ with respect to the [0,1,0] direction of the substrate. The in-plane anisotropy of the critical current density, of about one order of magnitude, has been explained by considering the anisotropy in the coherence length ξ and London penetration depth λ_L. The anisotropy ratios λ_c/λ_b and ξ_b/ξ_c have been consistently obtained from two independent measurements: critical current modulation depth of Dayem bridge nanoSQUIDs as a function of an externally applied magnetic field, and

broadening of the superconducting transition, due to vortex entry. Finally, we have studied the phase dynamics of our nanowires, by applying microwave radiation. The c-axis oriented nanowires show half-integer Shapiro steps, which get suppressed after an ozone treatment, restoring a proper oxygen content into the nanostructures. Two possible reasons of the presence of the half-integer Shapiro-like steps in the more de-oxygenated nanowires are the weak Josephson coupling between adjacent copper oxide planes, and the existence of a $4e$ superfluid component, theoretically predicted in the underdoped region of HTS, which coexists with the conventional $2e$ one.

Nanostructures patterned on a-axis YBCO films represent the ideal choice to realize superconducting proximity based hybrid systems; in addition to this, our experiments also showed that they can lead to a better understanding of still unresolved phenomena in high critical temperature superconductors, as the effect of the confinement of the a-b planes or the appearance of the charge density wave order.

[1] J. B. Barner, C. T. Rogers, A. Inam, R. Ramesh, and S. Bersey, Appl. Phys. Lett. **59**, 742 (1991).
[2] A. Inam, C. T. Rogers, R. Ramesh, K. Remschnig,

L. Farrow, D. Hart, T. Venkatesan, and B. Wilkens, Appl. Phys. Lett. **57**, 2484 (1990).
[3] P. Lucignano, A. Mezzacapo, F. Tafuri, and A. Taglia-

cozzo, Phys. Rev. B **86**, 144513 (2012).

[4] B. Lu, K. Yada, A. A. Golubov, and Y. Tanaka, Phys. Rev. B **92**, 100503 (2015).

[5] F. Miletto Granozio, M. Salluzzo, U. S. di Uccio, I. Maggio-Aprile, and Ø. Fischer, Phys. Rev. B **61**, 756 (2000).

[6] D. M. Hwang, T. S. Ravi, R. Ramesh, S. Chan, C. Y. Chen, L. Nazar, X. D. Wu, A. Inam, and T. Venkatesan, Appl. Phys. Lett. **57**, 1690 (1990).

[7] M. Mukaida and S. Miyazawa, Jpn. J. Appl. Phys. **31**, 3317 (1992).

[8] W. Ito, S. Mahajan, Y. Yoshida, N. Watanabe, and T. Morishita, J. Mater. Res. **9**, 1625 (1994).

[9] P. Zhao, A. Ito, R. Tu, and T. Goto, Appl. Surf. Sci. **257**, 4317 (2011).

[10] M. Mukaida and S. Miyazawa, Appl. Phys. Lett. **63**, 999 (1993).

[11] Z. Trajanovic, I. Takeuchi, P. Warburton, C. Lobb, and T. Venkatesan, Physica C **265**, 79 (1996).

[12] J. Fujita, T. Yoshitake, A. Kamijo, T. Satoh, and H. Igarashi, J. Appl. Phys. **64**, 1292 (1988).

[13] N. Homma, S. Okayama, H. Takahashi, S. Kawamoto, I. Yoshida, M. Kamei, T. Morishita, T. Haga, and K. Yamaya, Physica C **194**, 430 (1992).

[14] A. Inam, R. Ramesh, C. T. Rogers, B. Wilkens, K. Remschnig, D. Hart, and J. Barner, IEEE Trans. Magn. **27**, 1603 (1991).

[15] Y.-S. He, P.-H. Wu, L.-F. Xu, Z.-X. Zhao, J. D. Suh, and G. Y. Sung, Physica C **282**, 579 (1997).

[16] Y. K. Park, D. H. Ha, K. Park, and J.-C. Park, Physica C **235**, 603 (1994).

[17] S. Hontsu, N. Mukai, J. Ishii, T. Kawai, and S. Kawai, Appl. Phys. Lett. **61**, 1134 (1992).

[18] S. Nawaz, R. Arpaia, F. Lombardi, and T. Bauch, Phys. Rev. Lett. **110**, 167004 (2013).

[19] R. Arpaia, S. Nawaz, F. Lombardi, and T. Bauch, IEEE Trans. Appl. Supercond. **23**, 1101505 (2013).

[20] A. Llordés, A. Palau, J. Gázquez, M. Coll, R. Vlad, A. Pomar, J. Arbiol, R. Guzmán, S. Ye, V. Rouco, F. Sandiumenge, S. Ricart, T. Puig, M. Varela, D. Chateigner, J. Vanacken, J. Gutiérrez, V. Moshchalkov, G. Deutscher, C. Magen, and X. Obradors, Nat. Mater. **11**, 329 (2012).

[21] J. Gutierrez, T. Puig, M. Gibert, C. Moreno, N. Rom, A. Pomar, and X. Obradors, Appl. Phys. Lett. **94**, 172513 (2009).

[22] J. C. Nie, H. Yamasaki, H. Yamada, Y. Nakagawa, K. Develos-Bagarinao, and Y. Mawatari, Supercond. Sci. Technol. **17**, 845 (2004).

[23] A. Frano, S. Blanco-Canosa, E. Schierle, Y. Lu, M. Wu, M. Bluschke, M. Minola, G. Christiani, H. U. Habermeier, G. Logvenov, Y. Wang, P. A. van Aken, E. Benckiser, E. Weschke, M. Le Tacon, and B. Keimer, Nat. Mater. **15**, 831 (2016).

[24] E. Berg, E. Fradkin, and S. A. Kivelson, Nat. Phys. **5**, 830 (2009).

[25] J. Chang, E. Blackburn, A. T. Holmes, N. B. Christensen, J. Larsen, J. Mesot, R. Liang, D. A. Bonn, W. N. Hardy, A. Watenphul, M. v. Zimmermann, E. M. Forgan, and S. M. Hayden, Nat. Phys. **8**, 871 (2012).

[26] C. B. Eom, A. F. Marshall, S. S. Laderman, R. D. Ja-

[27] cowitz, and T. H. Geballe, Science **249**, 1549 (1990).

[27] Z. Trajanovic, C. J. Lobb, M. Rajeswari, I. Takeuchi, C. Kwon, and T. Venkatesan, Phys. Rev. B **56**, 925 (1997).

[28] Y. Suzuki, D. Lew, A. Marshall, M. Beasley, and T. Geballe, Phy. Rev. B **48**, 10642 (1993).

[29] S. Tozer, A. Kleinsasser, T. Penney, D. Kaiser, and F. Holtzberg, Phys. Rev. Lett. **59**, 1768 (1987).

[30] T. Friedmann, M. Rabin, J. Giapintzakis, J. Rice, and D. Ginsberg, Phys. Rev. B **42**, 6217 (1990).

[31] J. Ye and K. Nakamura, Phys. Rev. B **48**, 7554 (1993).

[32] L. Bulaevskii, M. Graf, C. Batista, and V. Kogan, Phys. Rev. B **83**, 144526 (2011).

[33] R. Arpaia, D. Golubev, R. Baghdadi, M. Arzeo, G. Kunakova, S. Charpentier, S. Nawaz, F. Lombardi, and T. Bauch, Physica C **506**, 165 (2014).

[34] T. K. Worthington, W. J. Gallagher, and T. R. Dinger, Phys. Rev. Lett. **59**, 1160 (1987).

[35] J. Johansson, K. Cedergren, T. Bauch, and F. Lombardi, Phys. Rev. B **79**, 214513 (2009).

[36] M. Khapaev Jr, Supercond. Sci. Technol. **10**, 389 (1997).

[37] R. Arpaia, M. Arzeo, S. Nawaz, S. Charpentier, F. Lombardi, and T. Bauch, Appl. Phys. Lett. **104**, 072603 (2014).

[38] M. Arzeo, R. Arpaia, R. Baghdadi, F. Lombardi, and T. Bauch, J. Appl. Phys. **119**, 174501 (2016).

[39] R. Arpaia, S. Charpentier, R. Toskovic, T. Bauch, and F. Lombardi, Physica C **506**, 184 (2014).

[40] The small discrepancy at $0° < \gamma \leq 30°$ is due to the fact that part of the current, despite the orientation of the nanowires with $\gamma \neq 0°$, still flows along the b-axis ($\gamma = 0°$). This contribution is related to the presence of a-b planes, which cross the nanowire, connecting the two electrodes without any interruption. This happens up to an angle $\tilde{\gamma} = \tan^{-1}(w/L) \approx 33°$.

[41] G. Papari, F. Carillo, D. Stornaiuolo, D. Massarotti, L. Longobardi, F. Beltram, and F. Tafuri, Physica C **506**, 188 (2014).

[42] R. Baghdadi, R. Arpaia, S. Charpentier, D. Golubev, T. Bauch, and F. Lombardi, Phys. Rev. Applied **4**, 014022 (2015).

[43] G. Blatter, M. V. Feigel'man, V. B. Geshkenbein, A. I. Larkin, and V. M. Vinokur, Rev. Mod. Phys. **66**, 1125 (1994).

[44] R. Baghdadi, R. Arpaia, T. Bauch, and F. Lombardi, IEEE Trans. Appl. Supercond. **25**, 1 (2015).

[45] S. Nawaz, R. Arpaia, F. Lombardi, and T. Bauch, Phys. Rev. Lett. **110**, 167004 (2013).

[46] M.-H. Bae, R. C. Dinsmore III, T. Aref, M. Brenner, and A. Bezryadin, Nano Lett. **9**, 1889 (2009).

[47] S. Shapiro, Phys. Rev. Lett. **11**, 80 (1963).

[48] S. Shapiro, A. R. Janus, and S. Holy, Rev. Mod. Phys. **36**, 223 (1964).

[49] E. Berg, E. Fradkin, and S. A. Kivelson, Nat. Phys. **5**, 830 (2009).

[50] E. Fradkin, S. A. Kivelson, and J. M. Tranquada, Rev. Mod. Phys. **87**, 457 (2015).

[51] R. Kleiner, F. Steinmeyer, G. Kunkel, and P. Müller, Phys. Rev. Lett. **68**, 2394 (1992).